



Published in final edited form as:

Mol Biosyst. 2015 December ; 11(12): 3332–3346. doi:10.1039/c5mb00488h.

Computational modeling of cytokine signaling in microglia†

Warren D. Anderson^{a,b,c}, Hirenkumar K. Makadia^{a,c}, Andrew D. Greenhalgh^d, James S. Schwaber^{a,b,c}, Samuel David^d, and Rajanikanth Vadigepalli^{a,b,c}

^aDaniel Baugh Institute for Functional Genomics and Computational Biology, Sidney Kimmel Medical College, Thomas Jefferson University, Philadelphia, PA, USA

^bGraduate Program in Neuroscience, Jefferson College of Biomedical Sciences, Thomas Jefferson University, Philadelphia, PA, USA

^cDepartment of Pathology, Anatomy, and Cell Biology, Sidney Kimmel Medical College, Thomas Jefferson University, Philadelphia, PA, USA

^dCenter for Research in Neuroscience, The Research Institute of the McGill University Health Center, Montreal, Quebec, Canada

Abstract

Neuroinflammation due to glial activation has been linked to many CNS diseases. We developed a computational model of a microglial cytokine interaction network to study the regulatory mechanisms of microglia-mediated neuroinflammation. We established a literature-based cytokine network, including TNF α , TGF β , and IL-10, and fitted a mathematical model to published data from LPS-treated microglia. The addition of a previously unreported TGF β autoregulation loop to our model was required to account for experimental data. Global sensitivity analysis revealed that TGF β - and IL-10-mediated inhibition of TNF α was critical for regulating network behavior. We assessed the sensitivity of the LPS-induced TNF α response profile to the initial TGF β and IL-10 levels. The analysis showed two relatively shifted TNF α response profiles within separate domains of initial condition space. Further analysis revealed that TNF α exhibited adaptation to sustained LPS stimulation. We simulated the effects of functionally inhibiting TGF β and IL-10 on TNF α adaptation. Our analysis showed that TGF β and IL-10 knockouts (TGF β KO and IL-10 KO) exert divergent effects on adaptation. TGF β KO attenuated TNF α adaptation whereas IL-10 KO enhanced TNF α adaptation. We experimentally tested the hypothesis that IL-10 KO enhances TNF α adaptation in murine macrophages and found supporting evidence. These opposing effects could be explained by differential kinetics of negative feedback. Inhibition of IL-10 reduced early negative feedback that results in enhanced TNF α -mediated TGF β expression. We propose that differential kinetics in parallel negative feedback loops constitute a novel mechanism underlying the complex and non-intuitive pro- *versus* anti-inflammatory effects of individual cytokine perturbations.

†Electronic supplementary information (ESI) available. See DOI: 10.1039/c5mb00488h

Correspondence to: Rajanikanth Vadigepalli.

Introduction

Neuroinflammation is implicated in the pathophysiology of many disease conditions including Alzheimer's disease, epilepsy, stroke, traumatic brain injury, and infection. Microglia are the resident macrophages of the central nervous system (CNS) and these cells are key regulators of immune functions of the brain such as responses to bacterial infection, injury, or neurodegeneration.¹ Following an injury or inflammatory stimulus, microglia often adopt a non-ramified morphology and release a number of pro- and anti-inflammatory substances including cytokines and chemokines.²⁻⁵ At the extreme end of this continuum, microglia acquire an ameboid phenotype that supports mobilization to the lesion site for phagocytosis of damaged cellular material or pathogen.⁶⁻⁸ Microglia also express receptors for many secreted factors such that autocrine and paracrine signaling coordinate the inflammatory microenvironment in CNS parenchyma following glial activation.⁹ The morphological and neurochemical effects of glial activation can lead dysregulation of synaptic physiology and intrinsic neuronal excitability,¹⁰⁻¹⁵ thus highlighting the important functional implications of microglial activation. Furthermore, given the well established role of microglia in the development and maintenance of synaptic function,¹⁶⁻¹⁸ acute infection- or injury-driven microglial inflammation during development exerts chronic deleterious effects on CNS functions.¹⁹⁻²¹

It is well known that neuroinflammation often entails a complex panoply of interactions amongst neurons, astrocytes, endothelial cells, and various immune cells.^{22,23} However, microglia-mediated coordination of the inflammatory microenvironment is integral to the regulation of neuroinflammation.^{24,25} Despite the critical role of microglia in CNS homeostasis, the mechanisms regulating microglial inflammation are not well understood. Microglial secretion of pro-inflammatory cytokines is often considered to be harmful, although prevention of microglial activation has been shown to yield pathological consequences. For instance, antibodies directed against tumor necrosis factor- α (TNF α) have been shown to exacerbate multiple sclerosis, and mutations in a TNF α receptor gene have been shown to be associated with this disease.²⁶ Further, antiinflammatory cytokine interleukin-10 (IL-10) has been shown to produce inflammatory effects in the periphery.²⁷ Hence, understanding how dynamic interactions amongst cytokines coordinate the inflammatory microenvironment is an outstanding goal in neuroinflammation research.

It is clear that microglia both secrete and respond to a number of inflammatory cytokines.⁹ A expansive intracellular cytokine signaling network has been utilized in computational studies of microglia in Alzheimer's disease.^{28,29} However, a comprehensive network of microglial cytokine/chemokine autocrine/paracrine inter-cellular interactions has not been assembled to our knowledge. The elucidation of this network structure is necessary for defining the roles of secreted cytokines in coordinating processes such as cellular adaptation. Cells often adapt to a sustained stimulus by responding briefly and then returning to baseline, and this adaptation is supported by signaling network architectures involving negative feedback.³⁰ Bacterial toxin lipopolysaccharide (LPS) elicits TNF α release from cultured microglia followed by response adaptation in the continuous presence of the stimulus.³¹ TNF α has also been shown to stimulate negative feedback from IL-10 and transforming growth factor- β (TGF β).³¹⁻³³ While TNF α is an important component of the microglial innate immune

response, its adaptation to LPS is likely to be equally important for restraining inflammation and preventing unnecessary tissue damage. However, the mechanistic basis for TNF α adaptation, and the relative contributions of feedback inhibitors such as TGF β and IL-10 to adaptation, has not been established. Computational analyses have provided useful insight as to the mechanisms of adaptation.^{30,34} For instance, in a model of TLR-4-mediated NF κ B responses to LPS, occlusion of an anti-inflammatory negative feedback loop was counter-intuitively shown to enhance adaptation.³⁵ Such results highlight the value in studying the mutual influences of network structure and kinetics on system dynamics.³⁶

Many investigations of cytokine signaling in microglia examined the pairwise interactions between two cytokines, or the effects of one cytokine on a set of others.^{37,38} More comprehensive examinations of microglial phenotypic properties under varied inflammatory conditions, accomplished using next generation sequencing technologies,^{39,40} were limited to studies of few time points. Hence, we do not currently understand how the interplay amongst secreted cytokines, to which microglia are responsive, is coordinated to render physiological response characteristics such as adaptation. Furthermore, defining the interactions of the microglial cytokine network, as has been accomplished for astroglia,⁴¹ is necessary but insufficient for providing insight as to the control mechanisms that govern the physiological responses of the integrated network and the coordination of such responses over time.

Computational modeling approaches have provided valuable insights into the mechanisms of peripheral and CNS inflammatory regulation. Such models vary according to level of analysis, cell type specificity, and model formulation. Levels of analysis include intracellular biochemical signaling,⁴² autocrine/paracrine regulation of cell signaling, intercellular interactions,⁴³ global tissue level inflammatory regulation,^{44,45} and various multiscale models incorporating integrated levels of analysis.^{46–49} Intracellular signaling models are generally cell type-specific, where cell types include microglia^{28,42,50} and peripheral macrophage,^{51,52} as well as other cell types.^{53,54} Modeling formalisms range from Boolean logic representations²⁸ to differential equations^{42,51,54} and agent based models.^{46–48,55} We employed a novel computational approach to study microglial autocrine/paracrine cytokine interactions with a model characterized by differential equations. We focused on studying the LPS response in microglia. Simulations and analyses of our model revealed that TGF β and IL-10 have distinguishable kinetics and opposing contributions to adaptation of TNF α responses to LPS.

Experimental and computational methods

Mathematical model of autocrine/paracrine cytokine signaling in microglia

We employed a variant of the classic S-systems model formulation,⁵⁶ based on the successful application of such an approach in recent models incorporating cytokine–cytokine interactions.^{57,58} We used the following formulation to simulate the expression dynamics of each cytokine,

$$\begin{aligned}
\frac{dC_x}{dt} &= k_x f(C_i) f(C_j) - \gamma_x C_x - \gamma_{ss,x} C_{ss,x} \\
f(C_i) &= \left(\frac{\prod_i C_i (t - \tau_{d,ix})^{n_{ix}}}{\prod_i C_i (t - \tau_{d,ix})^{n_{ix}} + K_{ix}^{n_{ix}}} \right) \\
f(C_j) &= \left(\frac{K_{jx}^{n_{jx}}}{\prod_j C_j (t - \tau_{d,jx})^{n_{jx}} + K_{jx}^{n_{jx}}} \right) \\
C_{ss,x} &= C_x(t=0)
\end{aligned} \tag{1}$$

$$\gamma_{ss,x} = \frac{k_x \left(\prod_i \frac{C_{ss,i}^{n_{ix}}}{C_{ss,i}^{n_{ix}} + K_{ix}^{n_{ix}}} \right) \left(\prod_j \frac{K_{jx}^{n_{jx}}}{C_{ss,j}^{n_{jx}} + K_{jx}^{n_{jx}}} \right) - \gamma_x C_x}{C_{ss,x}} \tag{2}$$

where $C_x = C_x(t)$ is the expression of cytokine x (TNF α , IL-1 β , IL-6, TGF β , IL-10, or CCL5) that is produced at rate k_x upon activation by cytokine C_i at time $t - \tau_{d,ix}$. Thus, the delay term $\tau_{d,ix}$ is time between the activation of C_i and its subsequent activation of C_x . The activation of C_x depends on C_i according to a Hill function characterized by half-maximal activation constant K_{ix} and cooperativity coefficient n_{ix} . Similarly, inhibitory cytokine C_j reduces C_x production with time delay $\tau_{d,jx}$ according to a decreasing sigmoidal function characterized by K_{jx} and n_{jx} . The degradation of C_x occurred with both concentration-dependent and concentration-independent components determined by rate constants γ_x and $\gamma_{ss,x}$, respectively. The concentration-independent degradation term encompassed the initial value of cytokine x , which was set to $C_{ss,x} = 0.1$ for all cytokines, and a degradation constant that was set to maintain a constant steady state (eqn (2)) in the absence of stimulation.⁵⁹ According to available data, LPS directly stimulates the production of all species in our model aside from TGF β . Hence, LPS was included among the C_i terms for all species other than TGF β .

The model was implemented in MATLAB 2013a (The Math- Works Inc., Natick, MA) using *ode45* to integrate the differential equations. We found that *ode15s* gave approximately identical results. All parameter values appear in ESI[†] and code to implement the model is available on the modelDB database (<http://senselab.med.yale.edu/modeldb/>; accession number: 170029).⁶⁰

Parameter estimation

We followed a procedure similar to our previous work⁶¹ (see ESI[†] “Parameter estimation and model comparison” for further details). First, we initiated all coupling constants (K_{ix} and K_{jx}) based on available data. We then fitted the entire model parameter set to normalized experimental waveforms because our primary interest was to recapitulate the relative experimental kinetics (Fig. 1). Furthermore, it was not possible to fit our model to cytokine concentrations, given the available data, so the model was set in arbitrary units. We constrained the fits such that all model outputs were of the same order of magnitude (Fig.

[†]Electronic supplementary information (ESI) available. See DOI: 10.1039/c5mb00488h

S1, ESI[†]). The model includes a total of 93 parameters. We modeled cytokine interactions without explicitly incorporating mechanistic detail, hence, there is not an explicit relation between parameter values and biological mechanisms. In particular, our model is phenomenological and does not include details such as the dynamics of receptor–ligand interactions, intracellular signaling interactions, and gene expression regulation. Hence, it is not entirely appropriate to explicitly associate the model parameters with specific biological referents. Rather, each parameter aggregates a number of biological processes (*e.g.*, cytokine production rate depends on transcription, translation, and post-translational modification). As described in the ESI,[†] we used numerical optimization to fit parameters based on minimization of summed square differences between model prediction and experimental data. We implemented a global sensitivity analysis prior to selecting a final parameter set and manually tuned the most sensitive parameters, as well as parameter associated with the most sensitive network interactions (see Fig. 2 and 4D).

Global sensitivity analysis

We implemented variance-based global sensitivity analysis as described previously.^{61,62} We used the high dimensional model reduction technique to decompose model output variance with respect to parameter variations imposed across 100 000 samples. This implementation of global sensitivity analysis is superior in evaluating parameter sensitivity in terms of parameter sampling⁶³ and accurate performance on non-linear models.⁶⁴ The total contribution of parameter θ_j to C_x , including effects due to first and higher order interactions, was given by

$$S_{T_i} = \frac{E(V(C_x|\theta_{\sim i}))}{V(C_x)} = 1 - \frac{V(E(C_x|\theta_{\sim i}))}{V(C_x)} \quad (3)$$

where $E(\cdot)$ is the expectation of the argument and $V(C_x|\theta_{\sim i})$ is the variance of C_x conditioned on all parameters other than θ_i . We determined the global parametric sensitivities of the TNF α response to LPS by numerically estimating S_{T_i} for all model parameters according to a previously described algorithm.⁶² Two-fold variations were implemented for all parameters.⁶¹ See ESI[†] for further detail on sensitivity analyses and their implementation (“Sensitivity analyses”, Fig. S2 and S3).

Analysis of sensitivity to initial conditions

To assess the sensitivity of the LPS-mediated TNF α response to the initial conditions of anti-inflammatory cytokines TGF β and IL-10, we varied their initial values from 0.01 to 20 and evaluated the effects on the TNF α response. In addition, we performed all of these anti-inflammatory variations over the same range of initial TNF α values (TNF α_0). For these variations, we used 20 initial values from the aforementioned range, varied incrementally in log space. All combinations of TGF β , IL-10, and TNF α initial values were considered, thus generating 8000 simulations. To assess TNF α sensitivity, we computed the normalized gradient of the LPS-induced TNF α response with respect to either TGF β or IL-10 (see

Results, eqn (5) and (6)). We computed these gradients over a range of time points and TNF α_0 levels and plotted the data in a coordinate system defined by TGF β_0 and IL-10 $_0$.

Experimental techniques and data analysis

Animals—All procedures were approved by the Animal Care Committee of the Research Institute of the McGill University Health Centre (RIMUHC). Male homozygote IL-10 KO mice (obtained from Dr Radzioch, RIMUHC) or C57BL/6 control mice (WT; Charles River Laboratories, CA) at 8 to 12 weeks of age were used to obtain bone marrow derived macrophages for cell culture.

Macrophage culture and treatment—Macrophages were generated as previously described.⁶⁵ Briefly, mice were euthanized and their hind leg bones were removed. Bone marrow was flushed out, homogenized and red blood cells were hypotonically lysed. After washing, cells were cultured in RPMI media containing 10% fetal bovine serum (FBS; 10%, Invitrogen, CA), L-cell-conditioned media (10%; a source of M-CSF), penicillin/streptomycin, and vitamins solution (1%; Invitrogen, CA) for 7 days. Mature macrophages were re-plated at a density of 80 000 cells per well in 24-well plates and left to adhere overnight. Cells were treated with lipopolysaccharide (LPS; 100 ng mL⁻¹) or vehicle control (PBS) in RPMI containing FBS (10%) for 6 and 18 h durations.

Following LPS treatment, cells were lysed and total RNA was extracted using the RNeasy Lipid Tissue Kit (Qiagen, CA). Reverse-transcription was performed with the Omniscript Reverse Transcription Kit (Qiagen, CA), and qPCR was performed using 1 μ L of cDNA with Fast SYBR Green Master Mix (Applied Biosystems, CA) on a Step-One Plus qPCR machine (Applied Biosystems). Peptidylprolyl isomerase A (PPIA) was used as an internal control gene. TNF primer sequences for were as follows: forward: 5'-TTG CTC TGT GAA GGG AAT GG-3'; reverse: 5'-GGC TCT GAG GAG TAG ACA ATA AAG-3'.

Data analysis—We calculated TNF α expression following LPS application with standardization relative to PPIA. The effects of LPS on TNF α gene expression levels were computed as $-\Delta\Delta Ct$ values:⁶⁶

$$\begin{aligned}\Delta Ct_{\text{PBS}} &= Ct_{\text{TNF}\alpha, \text{PBS}} - Ct_{\text{PPIA}, \text{PBS}} \\ \Delta Ct_{\text{LBS}} &= Ct_{\text{TNF}\alpha, \text{LBS}} - Ct_{\text{PPIA}, \text{LBS}} \\ \Delta\Delta Ct &= \Delta Ct_{\text{LPS}} - \Delta Ct_{\text{PBS}}\end{aligned}$$

Statistical comparisons of LPS responses from WT *versus* IL-10 KO macrophages were performed using the two factor analysis of variance (ANOVA). The Tukey honestly significant difference (HSD) test was applied for multiple comparisons. The Mann-Whitney-Wilcoxon test was applied to check ANOVA results with a non-parametric test. Adaptation of the TNF α response to LPS from 6 to 18 h was computed as follows:

$$\text{Adaptation} = 1 - \left(\frac{\overline{-\Delta\Delta Ct_{18}}}{\overline{-\Delta\Delta Ct_6}} \right) \quad (4)$$

where $\overline{-\Delta\Delta Ct_i}$ represents the average gene expression change at time i . To compare adaptation between WT and KO genotypes, we used an ‘error propagation’ metric to estimate the standard deviation of adaptation:⁶⁷

$$\hat{\sigma} = \sqrt{\text{SEM}_6^2 \left(\frac{\partial A}{\partial(-\Delta\Delta Ct_6)} \right)^2 + \text{SEM}_{18}^2 \left(\frac{\partial A}{\partial(-\Delta\Delta Ct_{18})} \right)^2} \quad (5)$$

where $A = \text{Adaptation}$ (eqn (3)) and SEM_i is the standard error of the mean (*i.e.*, $\overline{-\Delta\Delta Ct}$) at time i . Statistical analyses were completed using functions *aov*, *TukeyHSD*, and *wilcox.test* in the statistical programming language R.⁶⁸

Results and discussion

Network structure and simulation of cytokine signaling in microglia

Our first goal was to establish a cytokine signaling network, based on microglial time-series data, that could be simulated with a mathematical model. Experimental data show the temporal profiles of cytokine release following the application of bacterial toxin lipopolysaccharide (LPS) to cultured microglia.⁶⁹ We created a network including the following cytokines/chemokines: TNF α , TGF β , IL-10, IL-6, IL-1 β , and chemokine (C–C motif) ligand 5 (CCL5). These species were chosen as network nodes for the following reasons: (1) there exist time-series data documenting the microglial release profile following LPS application for all network species, (2) a wealth of data exist with characterizations of the interactions amongst these cytokines (*e.g.*, the application of TGF β to LPS treated microglial cultures attenuates TNF α release³³), (3) these species are particularly relevant to our interest in CNS-mediated control over cardiovascular physiology, based on *in vitro* and *in vivo* data,^{70–72} and (4) these cytokines are of broad interest in neuroinflammation and neurodegenerative disease research.^{73–75}

We distilled the results of our literature search into the interaction network shown in Fig. 1A. All species in the network other than TGF β have been shown to be directly activated by LPS, while TGF β activation following LPS treatment depends on TNF α .⁷⁶ With one exception (see below), every edge in the network was derived from experimental data from microglia demonstrating an activating or inhibitory effect of the source node on the target (Table S1, ESI[†]). We assessed the topological properties of the network and found that TNF α exhibited connectivity features indicative of a prominent role in network control. TNF α had the highest in-degree, out-degree, and number of shortest path connections between other nodes. This suggests that TNF α is topologically situated to globally control the dynamics of the cytokine network, as expected based on experimental work.^{75,77–79}

To examine the dynamic coordination of microglial cytokine signaling, we developed a mathematical model based on the network of microglial cytokine/chemokine signaling interactions (Fig. 1A). A modified S-systems model formulation permitted calibration to experimental data (Fig. 1B).⁵⁶ A key assumption of our model formalism was that AND logical gating governs the combined effects of a group of cytokines on their target. For instance, if cytokines A and B both activate the production of cytokine C, cytokine C will only be produced if both A and B are active. In OR gating, if cytokines A and B both activate the production of cytokine C, cytokine C will be produced if either A and B is active. We attempted to implement OR gating, in which the sequence product operator was replaced by the summation operator in eqn (1), but the model could not be calibrated to data with this configuration (see ESI,[†] “OR gating model”). Hence, we hypothesize that AND gating characterizes the collective influences of a group of cytokines on their mutual target. We also assumed that the model rests at a steady-state state with arbitrarily low species levels in the absence of LPS. This assumption is consistent with data from cultured microglia in which cytokine expression is nearly undetectable in the absence of a perturbation,⁷⁶ and data suggest that the brain *in vivo* contains low cytokine levels under baseline conditions relative to disease states or responses to inflammatory stimuli.⁸⁰

While we did not find evidence in the published literature on microglia showing that TGF β coordinates its own release, we hypothesize the existence of this autoregulatory loop because its inclusion in our mathematical model was necessary to recapitulate the time-series data. Without the positive feedback autoregulation loop for TGF β , cytokine/chemokine data from experiments in which LPS was applied to cultured microglia could not be replicated by our model (Fig. 1B; see ESI,[†] “Experimental data used for parameter estimation” for further information). In particular, this autoregulation loop was necessary to obtain delayed and relatively slow LPS responses for TNF α , TGF β , and CCL5. Supporting the plausibility of this hypothesized TGF β autoregulatory loop, data from astrocytes (a CNS parenchymal cell-type involved in cytokine release with many functional similarities to microglia) show that TGF β application stimulates TGF β upregulation.^{41,81} TGF β autoregulation has also been demonstrated in the CNS *in vivo*,⁸² and in other non-CNS cell types.^{83–85} Our model prediction of similar TGF β autoregulation in microglia thereby yields a novel hypothesis for experimental evaluation. The final calibrated model recapitulated the relative experimental kinetics. These results suggest that our modeling formalism captures a complex set of interactions triggered by inflammatory stimulation by LPS.

In subsequent simulations, we found that our model with delay differential equations (DDEs, see Methods, eqn (1) and (2)) was computationally demanding to implement, and occasionally the model generated sharp deflections in the dynamic variables (see arrows in Fig. S1C; see also Fig. S10, ESI[†]). These sharp deflections were likely related to a numerical integration issue. However, DDEs did not provide a significant advantage, in terms of the model fit to data and model predictions, in comparison to ordinary differential equations (ODEs). To test whether we could obtain comparable results using ODEs, we set all time delay terms to zero ($\tau_d = 0$ in eqn (1)) and verified that the resulting ODE model yielded qualitatively similar simulation results (Fig. S1C, ESI[†]). Thus, even though the DDE model provided a better fit to data, the performance of the ODE model was optimal for our model analyses (see ESI,[†] “Parameter estimation and model comparison”, Tables S2 and

S3). The model fits appeared qualitatively similar and other simulation results were nearly identical for the ODE and DDE models. These results, along with others noted below, suggest that the DDE and ODE models are comparable. We examined the ODE model in the simulations and analyses presented below unless otherwise noted.

TNF α is sensitive to anti-inflammatory feedback inhibition

To determine the relative influences of model parameters on cytokine expression, we performed a global sensitivity analysis.^{61,62} This analysis entailed the variation of all parameters in tandem followed by the decomposition of model output variance into the relative contributions of each parameter. Because our initial analysis of the cytokine network revealed that TNF α is topologically positioned to exert robust control over network dynamics, and given the well documented role of TNF α in neuroinflammatory disease states,⁷⁵ we focused on the sensitivity of TNF α to the model parameters. Our sensitivity analysis showed that the TNF α response to sustained LPS input was most sensitive to parameters associated with TGF β production, IL-10 inhibition of TNF α , IL-1 β activation of TNF α , and IL-6 activation of IL-10 (Fig. 2). All other parameters had a relatively insignificant impact (*i.e.*, total sensitivity < 0.2) on the global variability of TNF α . Of all model parameters, 5.7% of the parameters exerted a prominent influence on the LPS-induced TNF α response, thereby indicating model robustness.

To enhance our confidence in model robustness and the absence of deleterious parameter uncertainty, we evaluated the first order sensitivity indices of each parameter and estimated the confidence bounds on the entire set of TNF α responses included in our global analysis. Furthermore, we conducted a local (*i.e.*, single parameter) sensitivity analysis and found independent validation of the results from our global analysis. The results from these analyses were consistent with model robustness (see ESI,[†] “Sensitivity analyses”, Fig. S2 and S3). To further address whether multiple parameter sets could predict the experimental data equally well, we performed parameter estimation starting from 20 randomly selected initial parameter sets (ESI,[†] “Parameter variation analyses”). The results show that several distinct parameter fits describe the data comparably, though none of the fits were significantly better than the reference parameter set (see Fig. S4A and Table S2, ESI[†]). These findings are thoroughly described and discussed in the ESI[†] (Fig. S4 and S5).

Endotoxin tolerance simulations support model validity

An important aspect of computational modeling is model validation using data that were not used for parameter estimation. Given that tolerance in the TNF α response to sequentially applied LPS stimuli has been experimentally observed in microglia,⁸⁶ we tested whether our model could recapitulate such endotoxin tolerance. Our results demonstrate that our model exhibits tolerance of the TNF α response to LPS over a range of inter-stimulus intervals (ISIs) and relative levels of the two LPS stimuli (Fig. 3B). To further examine the validity of our model, we tested whether TGF β regulated endotoxin tolerance, as was observed experimentally for microglia.⁸⁷ The relative effects of TGF β were isolated by simulating a functional knockout (KO) of this cytokine (*i.e.*, TGF β KO). This KO condition simulates the effect of pharmacological antagonism or genetic mutation. We found that TGF β KO enhanced response gain, thereby occluding tolerance (Fig. 3B). Our results

supported the experimental finding that TGF β enhanced tolerance of the TNF α response to LPS over a range of stimulus conditions. These results are consistent with model validity.

TNF α is prominently inhibited by kinetically distinct TGF β and IL-10 inputs

Our sensitivity analysis motivated us to further examine the relative influences of TGF β and IL-10 on TNF α . In agreement with the sensitivity analysis, experimental data suggest that TGF β and IL-10 are critical regulators of TNF α production in peripheral macrophages and microglia.^{88,89} Upon closer examination of the TGF β and IL-10 response profiles during LPS stimulation, we found that IL-10 activation temporally preceded TGF β activation (Fig. 4A). This temporal shift in the LPS-mediated activation of IL-10, relative to that of TGF β , resulted in an accelerated inhibitory input to TNF α from IL-10 compared to TGF β (Fig. 4). We evaluated the cumulative LPS-induced activation levels of TGF β and IL-10 by computing area under the expression curve (AUC) over time, as well as the relative contribution of total IL-10 expression (Fig. 4C). The results showed that IL-10 expression contributed more than 50% of the combined inhibitory input to TNF α throughout the upstroke, peak, and approximately half of the adapting decay in the continuous presence of LPS. Similar findings were obtained for the DDE model (Fig. S6, ESI[†]). Our results were not surprising given similar experimental findings.^{31–33,90} These results suggest that while IL-10 and TGF β jointly impose negative feedback on TNF α , the effects of IL-10 precede those of TGF β and play a greater role in shaping the peak TNF α response to LPS. Based on the above results, we chose to further investigate the relative contributions of IL-10 and TGF β to the regulation of TNF α . These interactions are highlighted in Fig. 4D.

A separatrix distinguishes anti-inflammatory initial condition effects on TNF α gradients

Because TGF β and IL-10 levels were believed to be particularly important for determining the TNF α response to LPS, we systematically evaluated the effects of initial TGF β , IL-10, and TNF α levels on the effects of continuously applied LPS. This analysis allowed us to assess the dependence of the TNF α response on the configuration of anti-inflammatory initial conditions. We simulated the LPS response for a set of permutations in the initial conditions of TNF α , TGF β , and IL-10. From these simulation results we computed the normalized TNF α gradients in the directions of both the TGF β and IL-10 initial levels (*i.e.*, TGF β_0 and IL-10 $_0$):

$$\nabla \text{TNF}\alpha|_{\text{TGF}\beta_0} = \frac{\partial \log \text{TNF}\alpha(t)}{\partial \log \text{TGF}\beta_0} \quad (6)$$

$$\nabla \text{TNF}\alpha|_{\text{IL}10_0} = \frac{\partial \log \text{TNF}\alpha(t)}{\partial \log \text{IL}10_0} \quad (7)$$

These gradients elucidate the sensitivity of the LPS-induced TNF α response changes in the initial conditions of either TGF β or IL-10. Further, these gradients showed how sensitivity to initial conditions varied depending on the relative baseline levels of TGF β and IL-10. Our

analysis entailed $\nabla \text{TNF}|_{\text{TGF}\beta_0}$ and $\nabla \text{TNF}|_{\text{IL}10_0}$ computations over a range of simulation times and $\text{TNF}\alpha_0$ values.

Our results revealed that the $\text{TNF}\alpha$ response to LPS declined with increases in the initial IL-10 level for particular pairings of the $\text{TGF}\beta$ and IL-10 initial expression levels (see blue bands in Fig. 5A). Combinations of the initial $\text{TGF}\beta$ and IL-10 levels along the diagonal of the $\text{TGF}\beta_0$ -IL-10₀ space rendered decreases in the $\text{TNF}\alpha$ response to LPS for increases in initial IL-10 levels when $\text{TNF}\alpha_0$ was relatively low (Fig. 5A; see Fig. S7, ESI[†] for similar plots of the $\text{TNF}\alpha$ gradient with respect to the initial $\text{TGF}\beta$ level). In addition to the negative $\text{TNF}\alpha$ response gradients for increases in IL-10₀ observed for certain combinations of the $\text{TGF}\beta$ and IL-10 initial levels, positive gradients were observed for other initial condition permutations (see red bands in Fig. 5A). $\nabla \text{TNF}|_{\text{IL}10_0} > 0$ occurred when increases in the initial IL-10 level led to increases in the $\text{TNF}\alpha$ response to LPS. The finding of such positive $\text{TNF}\alpha$ gradients with respect to IL-10₀ was surprising given that IL-10 inhibits $\text{TNF}\alpha$ expression and thus, increases in initial IL-10 levels would be expected to only reduce $\text{TNF}\alpha$ responses, as found for $\text{TGF}\beta$ (Fig. S7, ESI[†]). Hence, a separatrix defined by adjacent negative and positive gradients, extending along the negative diagonal of the $\text{TGF}\beta_0$ -IL-10₀ space, was observed for low $\text{TNF}\alpha_0$ values at simulation times around $t = 48$ h of LPS stimulation (Fig. 5A and B).

The evaluation of sample traces showed that the $\text{TNF}\alpha$ response amplitude and gradient varied inversely with respect to both $\text{TGF}\beta_0$ and IL-10₀ (Fig. 5B and C). We specifically examined the LPS-mediated $\text{TNF}\alpha$ response for a series of initial IL-10 levels at three levels of initial $\text{TGF}\beta$ (Fig. 5B). For the highest initial level of $\text{TGF}\beta$, increases in the initial amount of IL-10 resulted in decreases in the $\text{TNF}\alpha$ response amplitude, thereby producing the negative $\text{TNF}\alpha$ gradient with respect to IL-10₀ (Fig. 5C, top). At intermediate initial $\text{TGF}\beta$ levels, increased IL-10₀ resulted in reduced $\text{TNF}\alpha$ response amplitude along with a temporal shift in the response profile (Fig. 5C, middle). These temporal shifts in the $\text{TNF}\alpha$ response resulted in delays in both the response peaks and decays, the latter of which produced negative $\text{TNF}\alpha$ gradients with respect to initial IL-10 levels. Increasing IL-10₀ resulted in reduced kinetics of the LPS-mediated $\text{TNF}\alpha$ response. These responses were characterized by slower recovery from the peak and thus higher levels at late simulation times compared to the $\text{TNF}\alpha$ expression profile observed for lower initial IL-10 levels (Fig. 5C, middle). For the lowest $\text{TGF}\beta_0$ level, negative $\text{TNF}\alpha$ gradients were found for earlier time points and regions of $\text{TGF}\beta_0$ -IL-10₀ space, whereas positive gradients were observed at relatively later simulation times (Fig. 5C, bottom). Similar to the case for intermediate $\text{TGF}\beta_0$ levels, increases in initial levels of IL-10 resulted in peak reductions and temporally right-shifted $\text{TNF}\alpha$ response profiles. This shift yielded both negative and positive gradients with respect to IL-10₀. In general, as $\text{TGF}\beta_0$ was reduced, the $\text{TNF}\alpha$ response was larger with a faster decay.

To further elucidate the basis for the separatrix observed at low initial $\text{TNF}\alpha$ levels (Fig. 5B), we examined adjacent temporal profiles of $\text{TNF}\alpha$ and $\nabla \text{TNF}|_{\text{IL}10_0}$ at select zones in $\text{TGF}\beta_0$ -IL-10₀ space (Fig. 5D and E). For zone 1, the $\text{TNF}\alpha$ response to LPS was small due to high $\text{TGF}\beta_0$ and an incremental increase in IL-10₀ resulted in a modest peak reduction associated with a negative gradient at corresponding times (Fig. 5E). When both $\text{TGF}\beta_0$ and

IL-10₀ were high (zone 2), TNF α was unresponsive to LPS and this unresponsiveness was insensitive to changes in IL-10₀. In contrast, zone 3 was characterized by negative gradients at all time points, due to the moderately high levels of both TGF β ₀ and IL-10₀. In zone 4, the presence of negative gradients, temporally followed by positive gradients, resulted from the combined effects of reduced TNF α response amplitude and decrease in response kinetics (Fig. 5D and E). To further evaluate the effects of initial conditions on the network response, we performed a Lyapunov exponent analysis (see ESI,[†] “Lyapunov exponent analysis”). This analysis showed that regions of TGF β ₀–IL-10₀ space with the highest sensitivities to initial conditions corresponded to the negative gradients observed with low TNF α ₀ in Fig. 5A (Fig. S8, ESI[†]). This suggests that $\nabla \text{TNF}|_{\text{IL}10_0}$ is indicative of global network sensitivity under such conditions. Overall, these results show that the cytokine network is sensitive to initial antiinflammatory conditions. For low TNF α levels, a single negative TNF α gradient with respect to initial IL-10 expression temporally precedes the instantiation of a separatrix defined by adjacent negative and positive gradients in TGF β ₀–IL-10₀ space.

TGF β and IL-10 exert divergent effects on the adaptation of TNF α to LPS

The preceding analyses identified TGF β and IL-10 as critical regulators of TNF α and established that the effects of IL-10 on TNF α are instantiated before those of TGF β . We next examined the relative effects of TGF β and IL-10 on TNF α adaptation to sustained LPS stimulation. The relative effects of TGF β and IL-10 were isolated by simulating the KO of each cytokine (*i.e.*, TGF β KO and IL-10 KO). We simulated the responses to sustained LPS stimuli, over a concentration range, in wildtype (WT) and KO phenotypes (Fig. 6A–C). We computed adaptation based on the relative levels of the peak TNF α response and the TNF α level at $t = 3$ days of LPS stimulation (termed steady state response, Fig. 6D):

$$\text{Adaptation} = 1 - \left(\frac{\text{TNF}\alpha_{\text{steadystate}}}{\text{TNF}\alpha_{\text{peak}}} \right) \quad (8)$$

For the WT phenotype, the degree of TNF α adaptation exhibited a sigmoidal dose–response profile (Fig. 6E). For IL-10 KO, we observed increased adaptation (left-shifted adaptation curve), whereas TGF β KO produced a reduction in adaptation (right-shifted adaptation curve) (Fig. 6E). These results suggest that IL-10 reduces adaptation whereas TGF β enhances adaptation. Both KO phenotypes produced relatively shallow dose–response adaptation curves in comparison to the WT phenotype. Further analyses showed that although KO of both TGF β and IL-10 resulted in increased TNF α peak response levels, albeit to different degrees (Fig. 6F), the removal of TGF β increased TNF α steady state values to a greater extent than observed for IL-10 KO (Fig. 6G). These findings suggest that TGF β controls adaptation by reducing both the peak and steady state TNF α responses to LPS. In contrast, IL-10 reduces the TNF α peak but does not affect the steady state, and thus IL-10 reduces adaptation.

To further characterize the relative effects of TGF β and IL-10 on the TNF α response to LPS, we assessed the time from stimulus initiation to peak response (ttp) and area under the expression curve (AUC) for the three phenotypic conditions. We found that TGF β KO

increased ttp while IL-10 KO decreased ttp (Fig. 6H). This suggests that TGF β reduces ttp and thereby speeds up the peak TNF α response to LPS, whereas IL-10 delays the peak response. We examined the cumulative amounts of TNF α produced following the initiation of LPS stimulation by computing the TNF α integrals (AUCs) over time. The results showed that KO of either TGF β or IL-10 resulted in AUC increases. The TGF β KO phenotype resulted in a greater TNF α expression increase than that for IL-10 elimination at lower LPS levels, but the KO AUCs converged as LPS was increased. Similar findings for the effects of anti-inflammatory occlusion were obtained for the DDE model (Fig. S9, ESI[†]). These results suggest that TGF β occlusion may result in particularly harmful inflammatory effects at low levels of inflammatory stimulation, whereas the effects of IL-10 elimination may be exacerbated as a function of stimulus intensity.

Because TGF β appeared to enhance adaptation, we examined the TGF β amplitude following an LPS stimulus in WT and IL-10 KO phenotypes (Fig. S10A, ESI[†]). The TNF α peak was smaller for the WT phenotype in comparison to IL-10 KO. However, peak TNF α expression was positively related to TGF β in both phenotypes. This analysis showed that TGF β was activated in proportion to the degree of LPS-induced TNF α activation, which was attenuated by IL-10. Similarly, IL-10 expression was positively related to TNF α for WT and TGF β phenotypes (Fig. S10B, ESI[†]). Collectively, our data demonstrate that LPS-activated TNF α levels determine the amount of TGF β produced. In turn, TGF β determines the degree of tolerance. In contrast, IL-10 reduces the TNF α response and consequently the amount of TGF β produced following the LPS stimulus. Overall, these novel simulation results indicate that antiinflammatory cytokines TGF β and IL-10, which both provide feedback inhibition to TNF α , have surprisingly disparate effects on TNF α , related to temporal differences in expression and feedback regulation.

IL-10 attenuates TNF α adaptation to LPS in murine macrophages

To experimentally test the hypothesis that IL-10 suppresses adaptation of the TNF α response to LPS, we compared the LPS responses of macrophages isolated from WT and IL-10 KO mice. We evaluated TNF α expression using qPCR at six and 18 hours after the initiation of continuously applied LPS (100 ng mL⁻¹). We quantified the TNF α response to LPS by computing $-Ct$ values (Fig. 7A, see Methods). To compare the LPS responses in WT *versus* IL-10 KO macrophages, we performed a two factor ANOVA to determine the effects of genotype (WT, IL-10 KO), LPS stimulus duration (6, 18 h) and the corresponding interaction. Our results showed significant effects of LPS duration ($F=137.7$, $P=3.6 \times 10^{-7}$), genotype ($F=5.0$, $P=0.05$), and a duration/genotype interaction ($F=20.9$, $P=0.001$). A *post-hoc* analysis revealed that the mean TNF α response was not different at six h post LPS application in WT (mean = 5.33, sd = 0.97, $n=3$) compared to IL-10 KO (mean = 6.3, sd = 0.53, $n=4$; $P=0.40$). At 18 h, the TNF α expression responses were increased in WT (mean = 2.43, sd = 0.91, $n=4$) compared to IL-10 KO (mean = -0.26, sd = 0.23, $n=3$; $P=0.003$). Additionally, we examined the difference between WT and IL-10 KO TNF α expression at 18 h using the Mann–Whitney–Wilcoxon test, a non-parametric test of similarity between distributions. The results provided support for time-dependent genotype difference ($P=0.057$). These results show that although IL-10 KO does not affect the

macrophage TNF α response to six h LPS, IL-10 KO results in a reduced TNF α to LPS following 18 h of stimulation.

Our experimental data suggest that occluding IL-10-mediated negative feedback regulation of TNF α inhibits TNF α release following prolonged LPS application, though TNF α was not decreased by IL-10 KO at six h. This trend is consistent with IL-10-mediated repression of TNF α adaptation to LPS. To test whether IL-10 KO influences TNF α adaptation to LPS, we computed the degree of adaptation between six and 18 h of LPS stimulation for WT and IL-10 KO macrophages (Fig. 7B). We found that adaptation was reduced in WT compared to the IL-10 KO (WT adaptation = 0.54, IL-10 KO adaptation = 1.04, see Methods eqn (3)). To evaluate the errors of these adaptation calculations, we applied an error propagation computation to estimate the respective standard deviations of WT *versus* KO adaptation (Methods eqn (4)). Based on these estimated deviations, we computed the adaptation values \pm two times the standard deviations (adaptation $\pm 2 \times$ sd): for the WT genotype this interval was (0.35, 0.74) whereas for the IL-10 KO genotype the interval was (1.00, 1.08). The adaptation $\pm 2 \times$ sd intervals were non-overlapping and these intervals are likely to encompass the respective 95% confidence intervals ($\text{mean} \pm 2 \times \text{sd} / \sqrt{n}$). Thus, our results provide convincing evidence that IL-10 KO increases adaptation of TNF α to LPS. Our experimental results support our computationally derived hypothesis that IL-10-mediated inhibition of TNF α has the counter-intuitive effect of suppressing adaptation to LPS.

Discussion

Our microglial cytokine network was established based on controlled cell culture experiments that demonstrated pairwise functional interactions between cytokines. Network inference approaches have shown utility in generating network structures from large data sets,⁹¹ but we chose to restrict our analysis to only interactions that have been experimentally validated. Data driven network structures can lack biological precision due to spurious correlations, inadequate pruning of indirect connections, and lack of information on edge sign (activation *versus* inhibition).^{92–94} Our approach of using mechanistic interaction data sets obviated the need for network discovery approaches.

In our modeling approach, we implemented a mathematical framework derived from the S-systems formalism.⁵⁶ Similar adaptations of the S-systems model have been useful in previous models involving cytokine signaling.^{57,58,95,96} A key assumption of our model was that the integrated effects of input cytokines on their target are governed by AND gating. While we do not have specific evidence validating this assumption for all connections in the network, both computational and experimental data indicate that AND gating is common in intracellular signaling networks involved in coordinating cytokine responses and production.^{97–100} Furthermore, incubation of macrophages with either TGF β or IL-10 renders the cells almost completely refractory to LPS such that TNF α release is negligible,⁹⁰ consistent with AND gating. Thus we hypothesize that such AND gating characterizes microglial cytokine interactions based on the congruence between our model and the available kinetic data.

Our network included an inhibitory effect of IL-6 on TNF α based on experimental data showing that IL-6 attenuates TNF α production by cultured microglia in response to LPS.³¹ However, it has been shown that IL-6 activates latent TGF β ,¹⁰¹ and this interaction was not included in our network model. We did not include this interaction because our sensitivity analyses indicated that the interaction between IL-6 and TNF α did not significantly contribute to our simulation results. Furthermore, a number of well documented molecular species that were not included in our model have been shown to influence the microglial phenotype.¹⁰² In particular, interferon- γ , nitric oxide, and superoxide have been shown to regulate microglial inflammation,¹⁰² and these species have been shown to exert effects on TGF β regulation in other immune cells.^{103,104} While we appreciate that these interactions may be important in the context of microglial LPS response, we chose not to include such interactions based on the dearth of microglia-specific data regarding these regulatory mechanisms, and the lack of time-series data necessary for parameter estimation.

A common feature of many systems biology models is that the inverse problem of parameter estimation is ill posed such that multiple non-unique solutions exist, thus rendering the problem underdetermined.^{105,106} This problem can be mitigated by using regularization techniques to facilitate error reduction in parameter estimation.¹⁰⁷ However, the utilization of such techniques requires *a priori* criteria for penalizing certain parameter fits. It has been proposed that *a priori* information should not be used in solving inverse problems based on philosophical and mathematical arguments.¹⁰⁸ While confidence in a model is enhanced by confidence in parameter estimates and parameter identifiability,^{109,110} it has been demonstrated that many models in systems biology and other areas of science have a spectrum unidentifiable parameters with exceedingly large confidence bounds.^{106,111} Even with very large data sets, such “sloppy” parameters can be prohibitively difficult to precisely estimate experimentally.^{106,110} While lack of parameter precision is a limitation inherent to situations in which the number of parameters exceeds the number of experimental data points, as in our case, approaches have been devised to mitigate problems associated with model parameter inidentifiability. Such alternative approaches include focusing on the robustness of model predictions¹⁰⁶ and simulating a spectrum of parameter set phenotypes^{108,112} (see ESI,[†] “Parameter analysis discussion” for an expanded discussion). Our approach integrated the aforementioned perspectives by using sensitivity analysis to (1) focus manual parameter tuning of sensitive parameters, (2) thoroughly assess model output uncertainty, and (3) verify our model predictions for a population of optimized parameter sets. As detailed in the ESI,[†] we demonstrated that our model generates well constrained predictions. Thus, despite the limitation that our parameters are not ideally constrained, due to the lack of adequately sampled data, our predictions have very tight confidence bounds. The validity of our model is also supported by our findings of endotoxin tolerance and its dependence on TGF β . Furthermore, we have performed Differential Lyapunov exponent analysis for TNF α trajectory to examine the maximal exponential rate of divergence of trajectories surrounding it. Our results indicate that the negative feedback loops imposed by IL-10 and TGF β are more sensitive to perturbations in the initial state when the system is operating closer to the bifurcation point (Fig. 5B). Despite all the complexities in the network, the model preserves bifurcative characteristics of negative feedback loops as observed elsewhere.¹¹³ These results are consistent with our sensitivity analyses indicating

model robustness. Finally, our model predictions regarding tolerance and adaptation were confirmed in 5/7 (>70%) of parameter the parameter sets estimated from random starting points (Fig. S5, ESI[†]).

Topological analysis of our cytokine interaction network suggested that TNF α is a critical control-point for the microglial LPS response. Global sensitivity analysis of our mathematical model showed that TGF β and IL-10 are prominent feedback inhibitors of TNF α . Consistent with these analyses, TNF α has been implicated as a regulator of neuroinflammation in central infections^{77,78} and traumatic injuries² as well as neurological, neurodegenerative, and psychiatric diseases.^{75,79} Assessment of TNF α sensitivity to the initial state of the network showed that the initial levels of TGF β and IL-10 can exert opposing influences on TNF α . Increases in the initial levels of TGF β could only lead to reductions of the TNF α response to LPS regardless of the initial IL-10 and TNF α levels. However, increases in the initial levels of IL-10 could elicit TNF α peak reductions and temporal shifts. These results indicate the instance of a separatrix depending on the initial states of TGF β and IL-10. Based on our topological analysis of the network, and sensitivity analyses of the mathematical model, we focused our study on the roles of TGF β and IL-10 in regulating TNF α dynamics. While we did not explicitly examine the contributions of IL-1 β , IL-6, and CCL5 to network behavior in our simulations, their presence in the model shaped the network interactions we studied.

To further assess the functional implications of cytokine interaction dynamics, we studied the contributions of TGF β and IL-10 to TNF α expression in the physiological context of adaptation to LPS. Surprisingly, TGF β and IL-10 were found to have opposing effects on adaptation to LPS. These divergent effects appear to be related to the differences in the kinetics of the feedback inhibition. Experimental data from macrophages and microglia show that that IL-10 activation precedes that of TGF β .^{31-33,90} IL-10 controls the amount of TGF β produced by providing relatively fast negative feedback to TNF α and thereby coordinating its level of activation. In turn, TGF β regulates the sustained level of TNF α . Based on our modeling predictions, we experimentally tested the hypothesis that IL-10 KO results in enhanced TNF α adaptation to sustained LPS in macrophages. Our data supported the mechanisms proposed based on our modeling work, thereby demonstrating that IL-10 occlusion enhances adaptation to LPS. However, we note that our model predicts a relatively augmented TNF α in the IL-10 condition. This was not observed in our experiment, however, we believe this is because we may not have sampled at the time of the peak response. Furthermore, the LPS response kinetics are likely to be different between WT and IL-10 KO conditions. Experiments are currently underway to address these possibilities. Nevertheless, our experimental results are consistent with enhanced adaptation following prolonged LPS exposure, whereas instance of peak modulation will be addressed in future experiments.

While recent evidence has shown microglia, under homeostatic conditions, express a unique gene profile,^{40,114} microglia and peripherally derived macrophages share the majority of genes involved in the inflammatory response. In a functional context, LPS tolerance of the TNF α to sequentially applied LPS doses has been observed in both macrophages¹¹⁵ and microglia.⁸⁶ Our model validation results were consistent with these findings. Furthermore, TGF β was shown to mediate LPS tolerance in both macrophages¹¹⁵ and microglia,⁸⁷ and

our model recapitulated these results. Importantly, there is a wealth of data demonstrating that macrophages and microglia engage similar interactions amongst TNF α , TGF, and IL-10.^{87,89,90,115,116} Therefore, we believe the use of macrophages is highly relevant in this context and validates our unexpected finding that IL-10 reduces TNF α adaptation. This interpretation is consistent with the common use of bone marrow-derived cells as models of neuroinflammation, given the experimental accessibility of these cells.^{6,117,118} Furthermore, given the issues raised above modeling issues related to the sloppiness and indentifiability of model parameters, our macrophage results support the generalizability of our findings to other myeloid cell types. Efforts are currently focused on modeling and experimentally testing the effects of IL-10 KO on adaptation and tolerance in microglia *in vivo*.

Our novel findings that TGF β and IL-10 exert opposing effects on adaptation supports and extends the conclusions of several modeling studies. It has been shown that negative feedback loops with differential kinetics exert distinguishable influences in an oscillating network.¹¹⁹ In a model of peripheral immune response to LPS, it was shown that relatively slow *versus* fast anti-inflammatory activation led to sepsis.¹²⁰ Faster anti-inflammatory activation was associated with restoration to health.¹²⁰ In contrast, we found that the faster IL-10 response was associated with pro-inflammatory effects *via* indirect inhibition of TGF β mediated indirectly by TNF α . An important distinction between our microglial model and peripheral infection models¹²⁰ is that the peripheral models simulate cell to cell interactions, whereas our model is microglia-specific. As such, seemingly pro-inflammatory effects of adjustments to anti-inflammatory levels in peripheral models occur due to excessive reduction of the capacity of phagocytes to clear pathogens. This context is distinct from our study of autocrine/paracrine regulation of microglia *via* cytokine network dynamics.

Similarly, simulations with a computational model of NF κ B dynamics showed that kinetically distinct negative feedback inhibitors (A20 and I κ B α) exert differential influences on the TNF α response to LPS stimulation.³⁵ A20 KO resulted in an enhanced TNF α response to LPS. Response adaptation was increased, as with our finding that IL-10 KO increased adaptation. Further, I κ B α KO resulted in an increased A20 response, analogous to our finding that IL-10 KO resulted in increased TGF β expression. However, the increased expression of A20 was insufficient for attenuating the LPS response in the NF κ B model. The A20 anti-inflammatory response adapted rapidly compared to the sustained activation anti-inflammatory cytokines in our model, thus highlighting a key difference between the systems under study. Hence, while a number of previous studies document phenomena similar to our observations, in the contexts of multi-cellular interactions or isolated signaling pathways, our study provides novel insights into the roles of parallel negative feedback interactions involving cytokine signaling in microglia.

Conclusions

Our simulations and analyses show novel phenomena whereby TGF β and IL-10 exert opposing influences on TNF α . While our focus on LPS response directly pertains to the microglial endotoxin response, microglial phenotypes associated with bacterial infection have been shown to resemble those associated with neurodegenerative diseases.¹²¹ In particular, LPS activates inflammatory signaling through interaction with tolllike receptor-4,

which also activates sterile inflammation in hypoxic, ischaemic, and traumatic injuries.^{122–126} It is clear that macrophages and microglia exhibit a plethora of stimulus-specific phenotypic states,^{127,128} although the mechanisms underlying regulation of cytokine production share a common network regulatory basis in disparate inflammatory phenotypes.¹²⁷ Our study of microglial LPS responses may have broader implications regarding cytokine network interactions stimulated by other inflammatory ligands such as beta-amyloid and alpha-synuclein. Simulations and analysis of our model highlight novel hypotheses that can be addressed through experiments with cultured microglia using available tools for perturbing and measuring cytokines. Thus, our model of cytokine signaling in microglia offers utility in generating mechanistic hypotheses regarding the therapeutic applications of cytokine perturbations to treat conditions associated with neuroinflammation.

Supplementary Material

Refer to Web version on PubMed Central for supplementary material.

Acknowledgments

Thanks to Dr Lakshmi Kuttippurathu and Dan Cook for helpful discussion and advice. Thank you to the reviewers for thoughtful comments and suggestions for improvement. Thank you to Dr Radzioch (RIMUHC) for providing IL-10 KO mice. This study was supported by National Heart, Lung, and Blood Institute grant No. R01 HL111621 to RV and JSS; and Canadian Institute of Health Research grant (MOP-14828) to SD.

References

1. Rock RB, Gekker G, Hu S, Sheng WS, Cheeran M, Lokensgard JR, Peterson PK. *Clin Microbiol Rev.* 2004; 17:942–964. [PubMed: 15489356]
2. Kroner A, Greenhalgh AD, Zarruk JG, Passos Dos Santos R, Gaestel M, David S. *Neuron.* 2014; 83:1098–1116. [PubMed: 25132469]
3. Parakalan R, Jiang B, Nimmi B, Janani M, Jayapal M, Lu J, Tay SSW, Ling EA, Dheen ST. *BMC Neurosci.* 2012; 13:64. [PubMed: 22697290]
4. David S, Kroner A. *Nat Rev Neurosci.* 2011; 12:388–399. [PubMed: 21673720]
5. Kettenmann H, Hanisch UK, Noda M, Verkhratsky A. *Physiol Rev.* 2011; 91:461–553. [PubMed: 21527731]
6. Greenhalgh AD, David S. *J Neurosci.* 2014; 34:6316–6322. [PubMed: 24790202]
7. Nimmerjahn A, Kirchhoff F, Helmchen F. *Science.* 2005; 308:1314–1318. [PubMed: 15831717]
8. Olson JK, Miller SD. *J Immunol.* 2004; 173:3916–3924. [PubMed: 15356140]
9. Hanisch UK. *Glia.* 2002; 40:140–155. [PubMed: 12379902]
10. Trapp BD, Wujek JR, Criste GA, Jalabi W, Yin X, Kidd GJ, Stohlman S, Ransohoff R. *Glia.* 2007; 55:360–368. [PubMed: 17136771]
11. Chen Z, Jalabi W, Hu W, Park HJ, Gale JT, Kidd GJ, Bernatowicz R, Gossman ZC, Chen JT, Dutta R, Trapp BD. *Nat Commun.* 2014; 5:4486. [PubMed: 25047355]
12. Riazi K, Galic MA, Kuzmiski JB, Ho W, Sharkey KA, Pittman QJ. *Proc Natl Acad Sci U S A.* 2008; 105:17151–17156. [PubMed: 18955701]
13. Pickering M, Cumiskey D, O'Connor JJ. *Exp Physiol.* 2005; 90:663–670. [PubMed: 15944202]
14. Stellwagen D, Malenka RC. *Nature.* 2006; 440:1054–1059. [PubMed: 16547515]
15. Pribiag H, Stellwagen D. *J Neurosci.* 2013; 33:15879–15893. [PubMed: 24089494]
16. Paolicelli RC, Bolasco G, Pagani F, Maggi L, Scianni M, Panzanelli P, Giustetto M, Ferreira TA, Guiducci E, Dumas L, Ragozzino D, Gross CT. *Science.* 2011; 333:1456–1458. [PubMed: 21778362]

17. Parkhurst CN, Yang G, Ninan I, Savas JN, Yates JR, Lafaille JJ, Hempstead BL, Littman DR, Gan WB. *Cell*. 2013; 155:1596–1609. [PubMed: 24360280]
18. Schafer DP, Lehrman EK, Stevens B. *Glia*. 2013; 61:24–36. [PubMed: 22829357]
19. Williamson LL, Sholar PW, Mistry RS, Smith SH, Bilbo SD. *J Neurosci*. 2011; 31:15511–15521. [PubMed: 22031897]
20. Bilbo SD, Biedenkapp JC, Der-Avakian A, Watkins LR, Rudy JW, Maier SF. *J Neurosci*. 2005; 25:8000–8009. [PubMed: 16135757]
21. Hornig M, Weissenbock H, Horscroft N, Lipkin WI. *Proc Natl Acad Sci U S A*. 1999; 96:12102–12107. [PubMed: 10518583]
22. Neher JJ, Brown GC. *Biochem Soc Trans*. 2007; 35:1166–1167. [PubMed: 17956303]
23. Barone FC, Feuerstein GZ. *J Cereb Blood Flow Metab*. 1999; 19:819–834. [PubMed: 10458589]
24. Saijo K, Glass CK. *Nat Rev Immunol*. 2011; 11:775–787. [PubMed: 22025055]
25. Welser-Alves JV, Milner R. *Neurochem Int*. 2013; 63:47–53. [PubMed: 23619393]
26. Gregory AP, Dendrou CA, Attfield KE, Haghikia A, Xifara DK, Butter F, Poschmann G, Kaur G, Lambert L, Leach OA, Prömel S, Punwani D, Felce JH, Davis SJ, Gold R, Nielsen FC, Siegel RM, Mann M, Bell JI, McVean G, Fugger L. *Nature*. 2012; 488:508–511. [PubMed: 22801493]
27. Mocellin S, Panelli MC, Wang E, Nagorsen D, Marincola FM. *Trends Immunol*. 2003; 24:36–43. [PubMed: 12495723]
28. Anastasio TJ. *Mol Biosyst*. 2015; 11:434–453. [PubMed: 25406664]
29. Anastasio TJ. *Front Pharmacol*. 2015; 6:116. [PubMed: 26097457]
30. Ma W, Trusina A, El-Samad H, Lim WA, Tang C. *Cell*. 2009; 138:760–773. [PubMed: 19703401]
31. Chao CC, Hu S, Sheng WS, Peterson PK. *Dev Neurosci*. 1995; 17:97–105. [PubMed: 7555742]
32. Sheng WS, Hu S, Kravitz FH, Peterson PK, Chao CC. *Clin Diagn Lab Immunol*. 1995; 2:604–608. [PubMed: 8548541]
33. Chao CC, Hu S, Sheng WS, Tsang M, Peterson PK. *Clin Immunol Immunopathol*. 1995; 77:358–365. [PubMed: 7586747]
34. Behar M, Hao N, Dohleman HG, Elston TC. *Biophys J*. 2007; 93:806–821. [PubMed: 17513354]
35. An GC, Faeder JR. *Math Biosci*. 2009; 217:53–63. [PubMed: 18835283]
36. Barzel B, Barabasi AL. *Nat Phys*. 2013; 9:673–681.
37. Minogue AM, Barrett JP, Lynch MA. *J Neuroinflammation*. 2012; 9:126. [PubMed: 22697788]
38. Hopp SC, Royer S, Brothers HM, Kaercher RM, D'Angelo H, Bardou I, Wenk GL. *J Neuroimmunol*. 2014; 267:86–91. [PubMed: 24393520]
39. Zhang Y, Chen K, Sloan SA, Bennett ML, Scholze AR, O'Keefe S, Phatnani HP, Guarnieri P, Caneda C, Ruderisch N, Deng S, Liddelow SA, Zhang C, Daneman R, Maniatis T, Barres BA, Wu JQ. *J Neurosci*. 2014; 34:11929–11947. [PubMed: 25186741]
40. Butovsky O, Jedrychowski MP, Moore CS, Cialic R, Lanser AJ, Gabriely G, Koeglsperger T, Dake B, Wu PM, Doykan CE, Fanek Z, Liu L, Chen Z, Rothstein JD, Ransohoff RM, Gygi SP, Antel JP, Weiner HL. *Nat Neurosci*. 2014; 17:131–143. [PubMed: 24316888]
41. Dong Y, Benveniste EN. *Glia*. 2001; 36:180–190. [PubMed: 11596126]
42. Sheppard PW, Sun X, Emery JF, Giffard RG, Khammash M. *BMC Bioinf*. 2011; 12:276.
43. Puri IK, Li L. *PLoS One*. 2010; 5:e15176. [PubMed: 21179474]
44. Rodriguez-Fernandez M, Grosman B, Yuraszcek TM, Helwig BG, Leon LR, Doyle FJ III. *PLoS One*. 2013; 8:e73393. [PubMed: 24039931]
45. Yiu HH, Graham AL, Stengel RF. *PLoS One*. 2012; 7:e45027. [PubMed: 23049677]
46. Marino S, Cilfone NA, Mattila JT, Linderman JJ, Flynn JL, Kirschner DE. *Infect Immun*. 2015; 83:324–338. [PubMed: 25368116]
47. Cilfone NA, Perry CR, Kirschner DE, Linderman JJ. *PLoS One*. 2013; 8:e68680. [PubMed: 23869227]
48. Ziraldo C, Mi Q, An G, Vodovotz Y. *Adv Wound Care*. 2013; 2:527–537.
49. Nguyen TT, Calvano SE, Lowry SF, Androulakis IP. *PLoS One*. 2013; 8:e55550. [PubMed: 23383223]

50. Sheppard PW, Sun X, Khammash M, Giffard RG. *PLoS Comput Biol.* 2014; 10:e1003471. [PubMed: 24516376]
51. Maiti S, Dai W, Alaniz R, Hahn J, Jayaraman A. *Processes.* 2014; 3:1–18.
52. Caldwell AB, Cheng Z, Vargas JD, Birnbaum HA, Hoffmann A. *Genes Dev.* 2014; 28:2120–2133. [PubMed: 25274725]
53. Moya C, Huang Z, Cheng P, Jayaraman A, Hahn J. *IET Syst Biol.* 2011; 5:15. [PubMed: 21261398]
54. Werner SL, Barken D, Hoffmann A. *Science.* 2005; 309:1857–1861. [PubMed: 16166517]
55. Correnti JM, Cook D, Aksamitiene E, Swarup A, Ogunnaike B, Vadigepalli R, Hoek JB. *J Physiol.* 2015; 593:365–383. [PubMed: 25630259]
56. Savageau MA. *J Theor Biol.* 1969; 25:370–379. [PubMed: 5387047]
57. Meyer-Hermann M, Figge MT, Straub RH. *Arthritis Rheum.* 2009; 60:2585–2594. [PubMed: 19714618]
58. Valeyev NV, Hundhausen C, Umezawa Y, Kotov NV, Williams G, Clop A, Ainali C, Ouzounis C, Tsoka S, Nestle FO. *PLoS Comput Biol.* 2010; 6:e1001024. [PubMed: 21152006]
59. Furchtgott LA, Chow CC, Perival V. *Biophys J.* 2009; 96:3926–3935. [PubMed: 19450465]
60. Hines ML, Morse T, Migliore M, Carnevale NT, Shepherd GM. *J Comput Neurosci.* 2004; 17:7–11. [PubMed: 15218350]
61. Miller GM, Ogunnaike BA, Schwaber JS, Vadigepalli R. *BMC Syst Biol.* 2010; 4:171. [PubMed: 21167049]
62. Saltelli, A., Ratto, M., Andres, T., Campolongo, F., Cariboni, J., Gatelli, D., Saisana, M., Tarantola, S. *Global Sensitivity Analysis The Primer.* Wiley-Interscience; Hoboken, NJ: 2008.
63. Tarantola S, Becker W, Zeitz D. *Comput Phys Commun.* 2012; 183:1061–1072.
64. Yang J. *Environ Modell Softw.* 2011; 26:444–457.
65. Longbrake EE, Lai W, Ankeny DP, Popovich PG. *J Neurochem.* 2007; 102:1083–1094. [PubMed: 17663750]
66. Livak KJ, Schmittgen TD. *Methods.* 2001; 25:402–408. [PubMed: 11846609]
67. Tellinghuisen, J. *Methods in Cell Biology.* Correia, IJJ., William Detrich, H., editors. Vol. 84. Academic Press; 2008. p. 737-780.
68. R Development Core Team. *R: A Language and Environment for Statistical Computing.* R Foundation for Statistical Computing; Vienna, Austria: 2008.
69. Chao CC, Hu S, Close K, Choi CS, Molitor TW, Novick WJ, Peterson PK. *J Infect Dis.* 1992; 166:847–853. [PubMed: 1527422]
70. Agarwal D, Dange RB, Raizada MK, Francis J. *Br J Pharmacol.* 2013; 169:860–874. [PubMed: 23516971]
71. Zubcevic J, Waki H, Raizada MK, Paton JFR. *Hypertension.* 2011; 57:1026–1033. [PubMed: 21536990]
72. Wu KLH, Chan SHH, Chan JYH. *J Neuroinflammation.* 2012; 9:212. [PubMed: 22958438]
73. Heneka MT, Kummer MP, Latz E. *Nat Rev Immunol.* 2014; 14:463–477. [PubMed: 24962261]
74. Whitney NP, Eidem TM, Peng H, Huang Y, Zheng JC. *J Neurochem.* 2009; 108:1343–1359. [PubMed: 19154336]
75. McCoy MK, Tansey MG. *J Neuroinflammation.* 2008; 5:45. [PubMed: 18925972]
76. Chao CC, Hu S, Sheng WS, Tsang M, Peterson PK. *Clin Immunol Immunopathol.* 1995; 77:358–365. [PubMed: 7586747]
77. Szretter KJ, Samuel MA, Gilfillan S, Fuchs A, Colonna M, Diamond MS. *J Virol.* 2009; 83:9329–9338. [PubMed: 19587044]
78. Chen CJ, Ou YC, Chang CY, Pan HC, Liao SL, Chen SY, Raung SL, Lai CY. *Glia.* 2012; 60:487–501. [PubMed: 22144112]
79. Park KM, Bowers WJ. *Cell Signalling.* 2010; 22:977–983. [PubMed: 20096353]
80. Vitkovic L, Konsman JP, Bockaert J, Dantzer R, Homburger V, Jacque C. *Mol Psychiatry.* 2000; 5:604–615. [PubMed: 11126391]

81. Cambier S, Gline S, Mu D, Collins R, Araya J, Dolganov G, Einheber S, Boudreau N, Nishimura SL. *Am J Pathol.* 2005; 166:1883–1894. [PubMed: 15920172]
82. Morgan TE, Rozovsky I, Sarkar DK, Young-Chan CS, Nichols NR, Laping NJ, Finch CE. *Neuroscience.* 2000; 101:313–321. [PubMed: 11074155]
83. Norgaard P, Spang-Thomsen M, Poulsen HS. *Br J Cancer.* 1996; 73:1037–1043. [PubMed: 8624260]
84. Joyce ME, Roberts AB, Sporn MB, Bolander ME. *J Cell Biol.* 1990; 110:2195–2207. [PubMed: 2351696]
85. Van Obberghen-Schilling E, Roche NS, Flanders KC, Sporn MB, Roberts AB. *J Biol Chem.* 1988; 263:7741–7746. [PubMed: 3259578]
86. Ajmone-Cat MA, Nicolini A, Minghetti L. *J Neurochem.* 2003; 87:1193–1203. [PubMed: 14622099]
87. Le Y, Iribarren P, Gong W, Cui Y, Zhang X, Wang JM. *J Immunol.* 2004; 173:962–968. [PubMed: 15240683]
88. Lodge PA, Sriram S. *J Leukocyte Biol.* 1996; 60:502–508. [PubMed: 8864135]
89. Bogdan C, Nathan C. *Ann N Y Acad Sci.* 1993; 685:713–739. [PubMed: 8363277]
90. Bogdan C, Paik J, Vodovotz Y, Nathan C. *J Biol Chem.* 1992; 267:23301–23308. [PubMed: 1429677]
91. Azhar N, Ziraldo C, Barclay D, Rudnick DA, Squires RH, Vodovotz Y. for the Pediatric Acute Liver Failure Study Group. *PLoS One.* 2013; 8:e78202. [PubMed: 24244295]
92. Zoppoli P, Morganella S, Ceccarelli M. *BMC Bioinf.* 2010; 11:154.
93. Janes KA, Lauffenburger DA. *Curr Opin Chem Biol.* 2006; 10:73–80. [PubMed: 16406679]
94. Kholodenko BN, Kiyatkin A, Bruggeman FJ, Sontag E, Westerhoff HV, Hoek JB. *Proc Natl Acad Sci U S A.* 2002; 99:12841–12846. [PubMed: 12242336]
95. Shao H, He Y, Li KCP, Zhou X. *Mol BioSyst.* 2013; 9:398–406. [PubMed: 23287963]
96. Ray JCJ, Wang J, Chan J, Kirschner DE. *J Theor Biol.* 2008; 252:24–38. [PubMed: 18321531]
97. Bezradica JS, Rosenstein RK, DeMarco RA, Brodsky I, Medzhitov R. *Nat Immunol.* 2014; 15:333–342. [PubMed: 24608040]
98. Saez-Rodriguez J, Alexopoulos LG, Epperlein J, Samaga R, Lauffenburger DA, Klamt S, Sorger PK. *Mol Syst Biol.* 2009; 5:331. [PubMed: 19953085]
99. Cheng CS, Feldman KE, Lee J, Verma S, Huang DB, Huynh K, Chang M, Ponomarenko JV, Sun SC, Benedict CA, Ghosh G, Hoffmann A. *Sci Signaling.* 2011; 4:ra11.
100. Morris MK, Saez-Rodriguez J, Clarke DC, Sorger PK, Lauffenburger DA. *PLoS Comput Biol.* 2011; 7:e1001099. [PubMed: 21408212]
101. Villiger PM, Kusari AB, ten Dijke P, Lotz M. *J Immunol.* 1993; 151:3337–3344. [PubMed: 8376781]
102. Vincent VA, Tilders FJ, Van Dam AM. *Mediators Inflammation.* 1998; 7:239–255.
103. Vodovotz Y, Chesler L, Chong H, Kim SJ, Simpson JT, DeGraff W, Cox GW, Roberts AB, Wink DA, Barcellos-Hoff MH. *Cancer Res.* 1999; 59:2142–2149. [PubMed: 10232601]
104. Vodovotz Y, Bogdan C, Paik J, Xie QW, Nathan C. *J Exp Med.* 1993; 178:605–613. [PubMed: 7688028]
105. Klipp, E., Liebermeister, W., Wierling, C., Kowald, A., Lehrach, H., Herwig, R. *Systems Biology.* John Wiley & Sons; 2011.
106. Gutenkunst RN, Waterfall JJ, Casey FP, Brown KS, Myers CR, Sethna JP. *PLoS Comput Biol.* 2007; 3:1871–1878. [PubMed: 17922568]
107. Engl HW, Flamm C, Kügler P, Lu J, Müller S, Schuster P. *Inverse Probl.* 2009; 25:123014.
108. Tarantola A. *Nat Phys.* 2006; 2:492–494.
109. Dai W, Bansal L, Hahn J, Word D. *AIChE J.* 2014; 60:181–192.
110. Raue A, Karlsson J, Saccomani MP, Jirstrand M, Timmer J. *Bioinformatics.* 2014; 30:1440–1448. [PubMed: 24463185]
111. Machta BB, Chachra R, Transtrum MK, Sethna JP. *Science.* 2013; 342:604–607. [PubMed: 24179222]

112. Daun S, Rubin J, Vodovotz Y, Roy A, Parker R, Clermont G. *J Theor Biol.* 2008; 253:843–853. [PubMed: 18550083]
113. Cai S, Zhou P, Liu Z. *Cogn Neurodyn.* 2013; 7:417–429. [PubMed: 24427216]
114. Hickman SE, Kingery ND, Ohsumi TK, Borowsky ML, Wang L-c, Means TK, El Khoury J. *Nat Neurosci.* 2013; 16:1896–1905. [PubMed: 24162652]
115. Pan H, Ding E, Hu M, Lagoo AS, Datto MB, Lagoo-Deenadayalan SA. *J Immunol.* 2010; 184:5502–5509. [PubMed: 20404275]
116. Naiki Y, Michelsen KS, Zhang W, Chen S, Doherty TM, Arditi M. *J Biol Chem.* 2005; 280:5491–5495. [PubMed: 15623538]
117. Vereyken EJF, Heijnen PDAM, Baron W, de Vries EHE, Dijkstra CD, Teunissen CE. *J Neuroinflammation.* 2011; 8:58. [PubMed: 21615896]
118. Wang W, Hu D, Xiong H. *Glia.* 2008; 56:241–246. [PubMed: 18046732]
119. Hoffmann A, Levchenko A, Scott ML, Baltimore D. *Science.* 2002; 298:1241–1245. [PubMed: 12424381]
120. Reynolds A, Rubin J, Clermont G, Day J, Vodovotz Y, Bard Ermentrout G. *J Theor Biol.* 2006; 242:220–236. [PubMed: 16584750]
121. Amor S, Puentes F, Baker D, van der Valk P. *Immunology.* 2010; 129:154–169. [PubMed: 20561356]
122. Bell MT, Puskas F, Agoston VA, Cleveland JC, Freeman KA, Gamboni F, Herson PS, Meng X, Smith PD, Weyant MJ, Fullerton DA, Reece TB. *Circulation.* 2013; 128:S152–S156. [PubMed: 24030400]
123. Kilic U, Kilic E, Matter CM, Bassetti CL, Hermann DM. *Neurobiol Dis.* 2008; 31:33–40. [PubMed: 18486483]
124. Tang SC, Arumugam TV, Xu X, Cheng A, Mughal MR, Jo DG, Lathia JD, Siler DA, Chigurupati S, Ouyang X, Magnus T, Camandola S, Mattson MP. *Proc Natl Acad Sci U S A.* 2007; 104:13798–13803. [PubMed: 17693552]
125. Caso JR, Pradillo JM, Hurtado O, Lorenzo P, Moro MA, Lizasoain I. *Circulation.* 2007; 115:1599–1608. [PubMed: 17372179]
126. Kigerl KA, Lai W, Rivest S, Hart RP, Satoskar AR, Popovich PG. *J Neurochem.* 2007; 102:37–50. [PubMed: 17403033]
127. Xue J, Schmidt SV, Sander J, Draffehn A, Krebs W, Quester I, De Nardo D, Gohel TD, Emde M, Schmidleithner L, Ganesan H, Nino-Castro A, Mallmann MR, Labzin L, Theis H, Kraut M, Beyer M, Latz E, Freeman TC, Ulas T, Schultze JL. *Immunity.* 2014; 40:274–288. [PubMed: 24530056]
128. Perry VH, Cunningham C, Holmes C. *Nat Rev Immunol.* 2007; 7:161–167. [PubMed: 17220915]

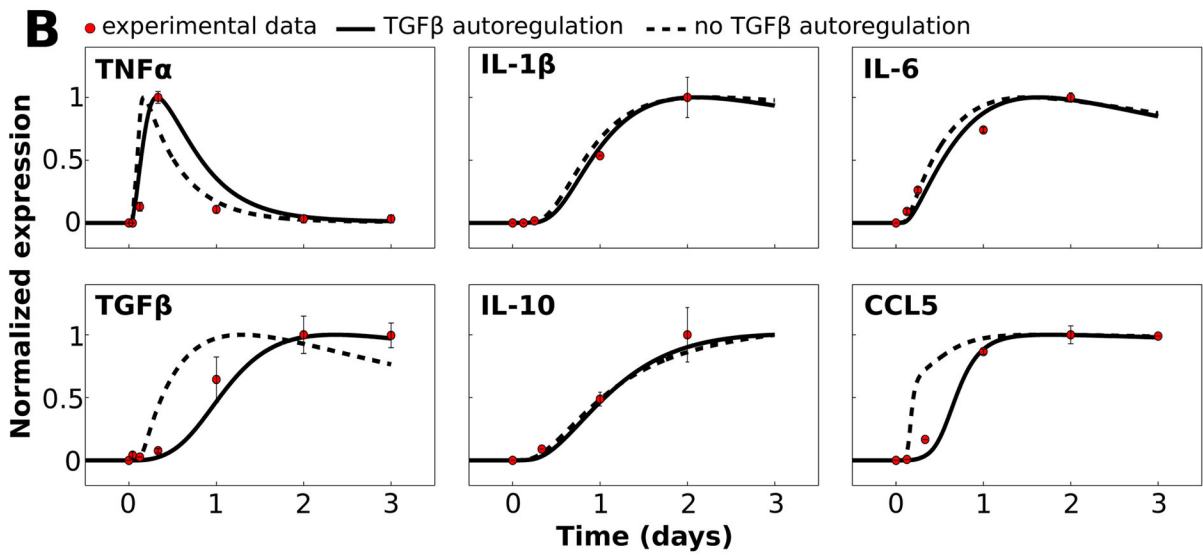
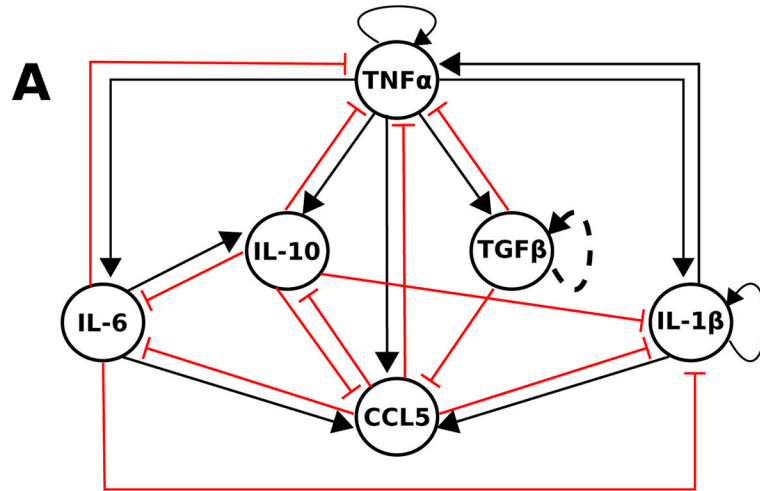


Fig. 1. Network model and mathematical simulation of complex signaling dynamics involving pro- and anti-inflammatory cytokines. (A) The literature-based network model depicts activation and inhibition of cytokine production, respectively, with black arrows and red T-connectors. The dashed line representing the TGF β autoregulation loop indicates that this interaction is hypothesized rather than demonstrated experimentally. All model species aside from TGF β were activated by LPS in our simulations. (B) The results of our calibrated model are shown along with normalized experimental kinetic profiles. Simulations were performed in which a saturating stimulus of LPS = 1000 was applied at $t = 0$ and maintained throughout the simulation. Traces are shown with and without the TGF β autoregulatory loop.

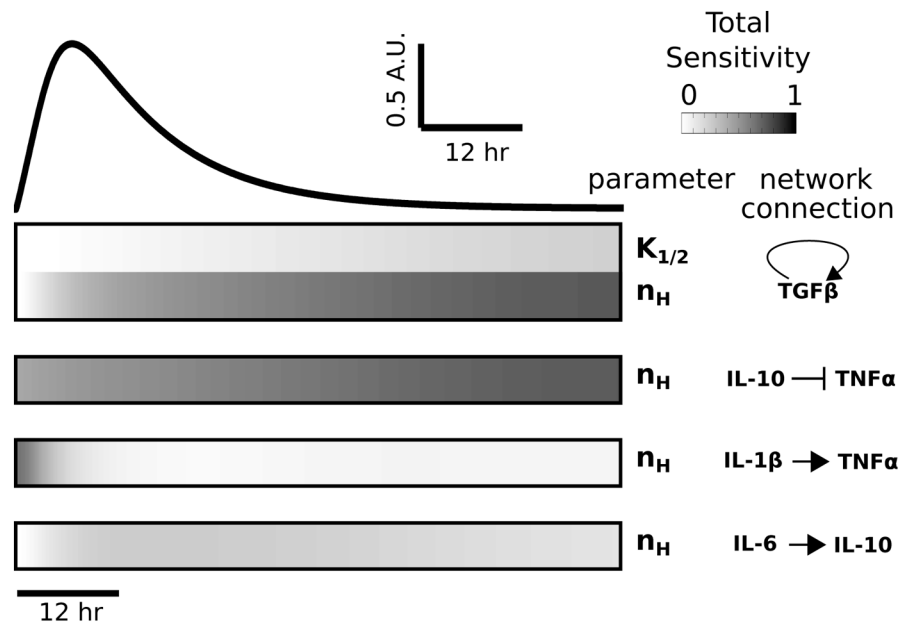


Fig. 2. Global sensitivity analysis reveals that $TNF\alpha$ is highly sensitive to $TGF\beta$ and $IL-10$. Total sensitivity indices (\mathcal{S}_T) were computed for each parameter and data are shown for all parameters with $\mathcal{S}_T > 0.2$. The temporal profile of the LPS-induced $TNF\alpha$ response, for saturating stimulus ($LPS = 1000$), is shown above the sensitivity index heatmap. Sensitivity indices were computed at times corresponding to the simulated waveform. All identified parameters involve one of the following cytokines: $IL-1\beta$, $TGF\beta$, $IL-10$, or $IL-6$.

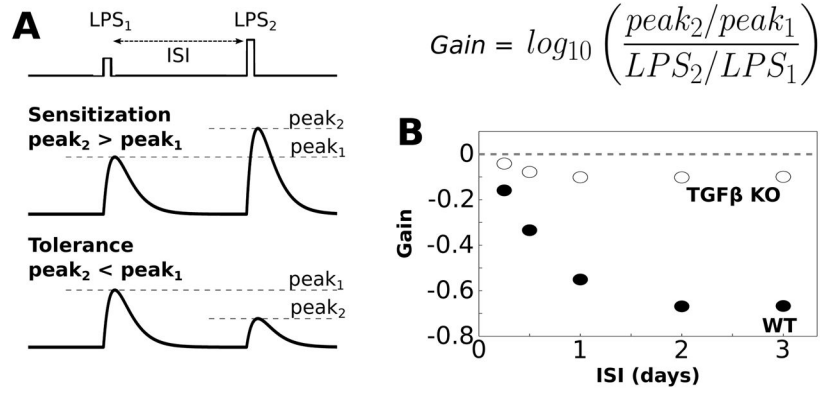


Fig. 3. Simulations of endotoxin tolerance support model validity. (A) Tolerance is evaluated by applying two sequential LPS doses, separated by an interstimulus interval (ISI), where the first dose is smaller than the second dose ($LPS_1 = 500$, $LPS_2 = 1000$). In general sensitization occurs when the peak response to the second LPS dose is greater than the peak response to the first dose ($gain > 0$, see equation). Tolerance occurs when the peak response to the second LPS dose is smaller than the peak response to the first dose ($gain < 0$). (B) Gain of the TNF α response to LPS was evaluated over a range of ISIs (2 h LPS pulse duration). For these simulations we set LPS = 0.1 during the ISI to maintain network coupling. Negative gain was observed for the wildtype condition for ISI > 6 h, thereby indicating tolerance. Simulated functional knockout (KO) of TGF β resulted in the absence of negative gain, thereby eliciting sensitization.

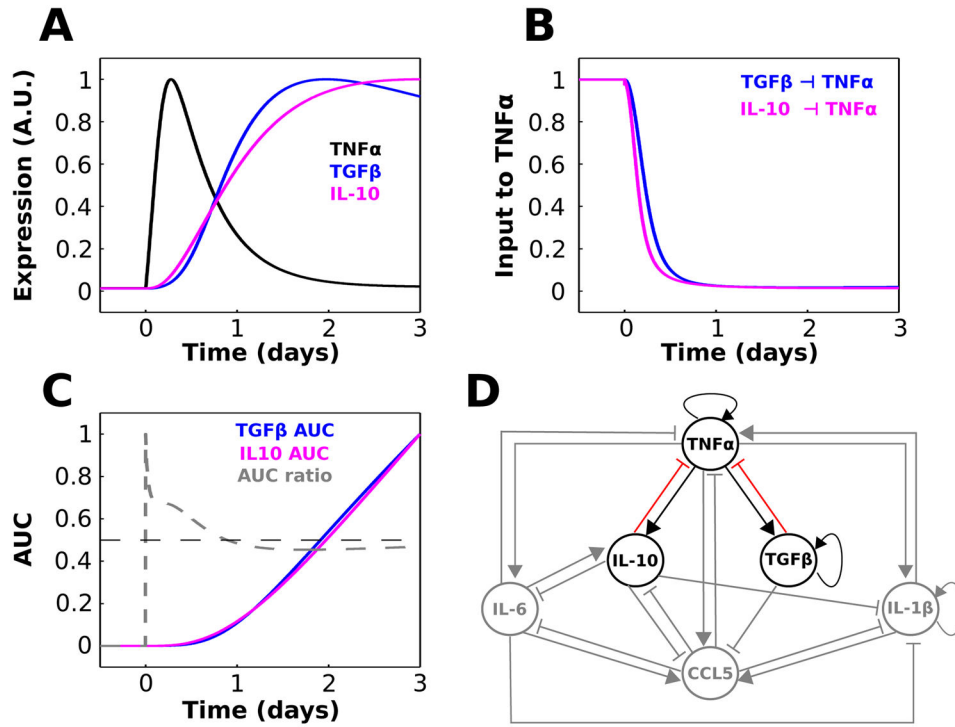


Fig. 4. TGFβ and IL-10 provide temporally distinct feedback inhibition to TNFα. (A) Relative waveforms of TNFα, TGFβ, and IL-10 are plotted for comparison (LPS = 1000 starting at $t = 0$). (B) Normalized TGFβ and IL-10 contributions to the TNFα activation rate equation show that IL-10-mediated inhibition of TNFα precedes that of TGFβ. These quantities were computed as $K_{TGF-TNF}^{n_{TGF-TNF}} / (TGF^{n_{TGF-TNF}} + K_{TGF-TNF}^{n_{TGF-TNF}})$ and $K_{IL10-TNF}^{n_{IL10-TNF}} / (IL10^{n_{IL10-TNF}} + K_{IL10-TNF}^{n_{IL10-TNF}})$. (C) Normalized area under the curve (AUC) was computed as a function of time for the TGFβ and IL-10 inputs to TNFα shown in panel A. The AUC ratio trace represents the fractional contribution of IL-10 relative to TGFβ: $AUC\ ratio = AUC_{IL10} / (AUC_{TGF} + AUC_{IL10})$. (D) Cytokine interaction network where sensitive interactions that will be the focus of the remainder of the paper are highlighted.

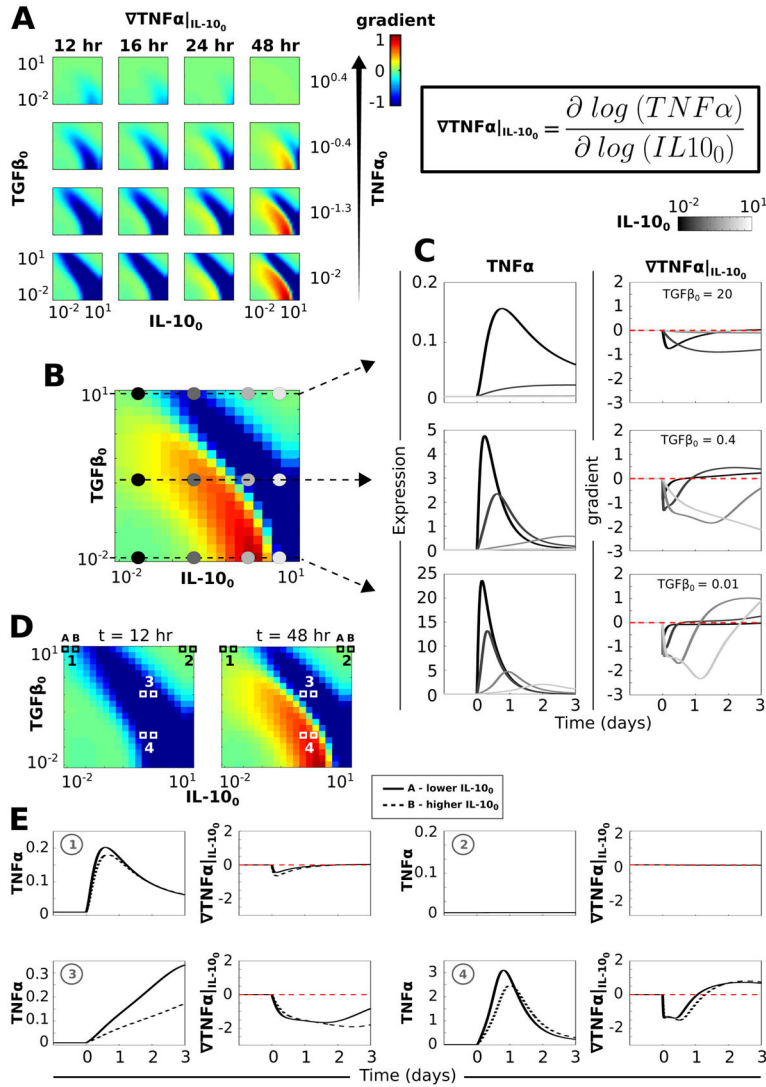


Fig. 5. A separatrix distinguishing $\text{TNF}\alpha$ response profiles exists in the $\text{TGF}\beta$ – IL-10 initial condition space. Simulations in which a saturating dose of $\text{LPS} = 1000$ was applied continuously starting at $t = 0$ were performed for range of $\text{TNF}\alpha$, $\text{TGF}\beta$, and IL-10 initial condition permutations. (A) The normalized $\text{TNF}\alpha$ gradient is plotted in the direction of the IL-10 initial condition (see equation in upper right). In each plot, the y -axis is defined by the $\text{TGF}\beta$ initial condition range and the x -axis is defined by the IL-10 initial condition range. Each column corresponds to a different time point at which the gradients were computed and each row corresponds to a different value of the initial $\text{TNF}\alpha$ level. (B) The plot shows the gradient for a low initial level of $\text{TNF}\alpha$ ($\text{TNF}\alpha_0 = 0.01$) at a late time point ($t = 48$ h). A separatrix cuts across the diagonal distinguishing negative *versus* positive gradients of the $\text{TNF}\alpha$ response to LPS with respect to increases in the initial IL-10 level. Colored circles denote the regions of initial condition space for which $\text{TNF}\alpha$ temporal profiles are shown in panel C. (C) Temporal profiles of $\text{TNF}\alpha$ (left) and $\nabla \text{TNF}\alpha|_{\text{IL-10}_0}$ (right) are shown for $\text{TNF}\alpha_0 = 0.01$ at three levels of $\text{TGF}\beta_0$ and four levels of IL-10_0 as indicated in panel B. (D)

Gradient plots for $\text{TNF}\alpha_0 = 0.01$ are shown at $t = 12$ h (left) and $t = 48$ h (right) along with numerical indicators of regions of $\text{TGF}\beta$ – IL-10 initial condition space examined in panel E. (E) Temporal profiles of $\text{TNF}\alpha$ and $\nabla\text{TNF}|_{\text{IL-10}_0}$ are shown for each of two adjacent values of IL-10_0 . This illustrates the correspondence between the temporal profile and computed gradient. Zone 1 in panel D is characterized by high $\text{TGF}\beta_0$ and low IL-10_0 . Increasing IL-10_0 from 0.01 to 0.15 resulted in a $\text{TNF}\alpha$ peak reduction associated with a negative gradient at corresponding times. Zone 2 depicts the $\text{TNF}\alpha$ gradients observed for relatively high initial $\text{TGF}\beta$ and IL-10 levels. Under these conditions, $\text{TNF}\alpha$ is unresponsive to LPS and the $\text{TNF}\alpha$ gradients are approximately zero. For zones 3 and 4, we compare the $\text{TNF}\alpha$ response to LPS at two adjacent IL-10_0 levels (1.2 and 1.8) at $\text{TGF}\beta_0$ levels on either side of the separatrix observed at 48 h. The data for zone 3, in which the $\text{TGF}\beta_0$ and IL-10_0 levels are relatively high (both 1.2), the $\text{TNF}\alpha$ response over three days of LPS stimulation is monotonically increasing and the gradient as a function of IL-10_0 is negative. If $\text{TGF}\beta_0$ is lowered to 0.07 (zone 4), the same increase in IL-10_0 results in a temporal shift in the $\text{TNF}\alpha$ profile along with a peak reduction. Due to the temporal shift, the gradient shows a negative deflection followed by a trajectory reversal into the positive range, thereby instantiating the positive gradient range demarcating the separatrix.

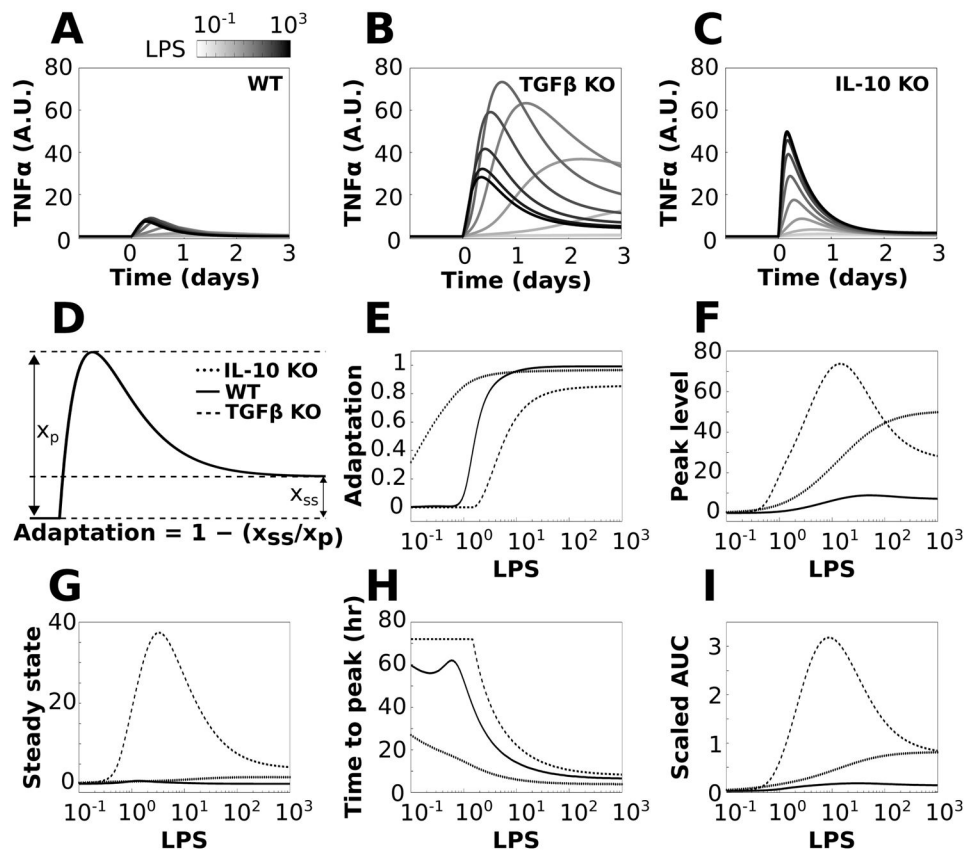


Fig. 6.

TGF β and IL-10 have divergent effects on TNF α adaptation. Simulations were performed for a range of LPS doses in which LPS was applied continuously starting at $t = 0$ for the duration of the simulation. The effects of knocking out TGF β or IL-10 were simulated by removing these nodes from the network. The reference simulation is referred to as WT and the knockouts are referred to as TGF β KO and IL-10 KO. (A–C) Sample TNF α responses to LPS are shown across the range of stimulation levels for the WT (A), TGF β KO (B), and IL-10 KO (C) phenotypes. (D) Adaptation was computed using the ratio of steady state to peak TNF α responses to sustained LPS applications (see equation). (E) Adaptation was computed for LPS inputs ranging from 0.1 to 1000 in all three model phenotypes. (F) Plots of maximal TNF α values show that KO of either feedback inhibitor increased the peak response to LPS. (G) The TNF α steady state response shows that TGF β knockout markedly increases the TNF α steady state, whereas IL-10 knockout has a relatively minor effect. (H) The time from the initiation of the LPS pulse to the peak TNF α response (ttp) is shown for the three conditions. (I) Plots show the total amount of TNF α produced following LPS application, assessed by the area under the TNF α curve (AUC).

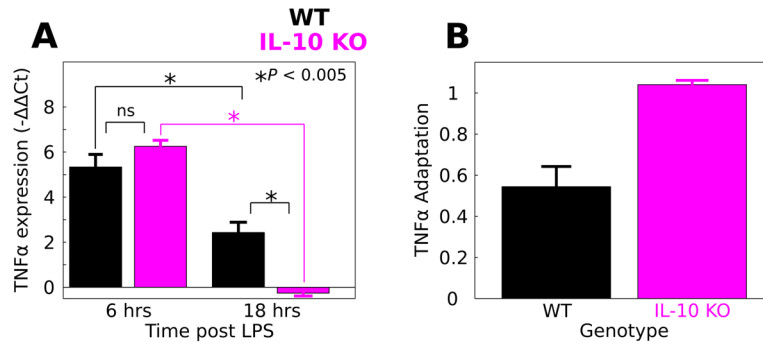


Fig. 7.

IL-10 restrains TNF α adaptation to LPS in macrophages. LPS was applied continuously to macrophage cultures from WT and IL-10 KO mice and TNF α gene expression was evaluated at 6 and 18 h stimulus durations. (A) IL-10 KO mice responded similarly to LPS applied for 6 h (data are presented as mean \pm SEM, * $P < 0.005$, ns – not significant). For 18 h of LPS stimulation, the IL-10 KO response was significantly attenuated relative to WT. (B) Adaptation was calculated for the WT and IL-10 KO macrophages based on the relative responses at 6 and 18 h (eqn (4)). Adaptation levels are shown along with corresponding estimates of standard deviation (eqn (5)). The analysis suggests that IL-10 KO enhances adaptation of the TNF α response to LPS in macrophages.